Nanoscale

PAPER

View Article Online
View Journal | View Issue

Optically enhanced charge transfer between C_{60} and single-wall carbon nanotubes in hybrid electronic devices†

Cite this: *Nanoscale*, 2014, **6**, 572

Christopher S. Allen,*[a] Guoquan Liu,[a] Yabin Chen,[b] Alex W. Robertson,[a] Kuang He,[a] Kyriakos Porfyrakis,[a] Jin Zhang,[b] G. Andrew D. Briggs[a] and Jamie H. Warner[a]

Received 14th August 2013
Accepted 4th November 2013

DOI: 10.1039/c3nr04314b

www.rsc.org/nanoscale

In this article we probe the nature of electronic interactions between the components of hybrid C_{60}–carbon nanotube structures. Utilizing an aromatic mediator we selectively attach C_{60} molecules to carbon nanotube field-effect transistor devices. Structural characterization *via* atomic force and transmission electron microscopy confirm the selectivity of this attachment. Charge transfer from the carbon nanotube to the C_{60} molecules is evidenced by a blue shift of the Raman G^+ peak position and increased threshold voltage of the transistor transfer characteristics. We estimate this charge transfer to increase the device density of holes per unit length by up to 0.85 nm^{-1} and demonstrate further optically enhanced charge transfer which increases the hole density by an additional 0.16 nm^{-1}.

Introduction

In order to fully exploit the potential of carbon nano-materials it is necessary to establish a comprehensive understanding of their interactions with other molecular species. Now that the fundamental physical properties of carbon nanotubes (CNTs) are relatively well understood,[1–3] attention is increasingly turning towards hybrid CNT–molecular systems.[4] Of primary concern for the development of CNT electronics is understanding how the presence of a particular molecule might affect conduction through a CNT and the mechanism behind this interaction.

Motivated primarily by the potential for chemical sensing applications, the effect of the physisorption of various molecules on the properties of nanotube field-effect transistors (CNTFETs) has recently been studied.[5–13] Changes in FET characteristics have been attributed to mechanisms such as charge-transfer doping[14] or Schottky barrier modulation.[5] However, for the development of complex hybrid CNT systems a more controllable functionalization process is required.

Both covalent and non-covalent routes are being explored for the robust and controllable functionalization of single-wall carbon nanotubes (SWCNTs).[15] Non-covalent functionalization is of particular interest as this should preserve the sp^2 lattice and consequently the excellent electronic properties of the host tube.[16] Pyrene groups have been shown to be an effective anchor for attaching compounds to SWCNTs[16–18] due to a strong π–π interaction between this aromatic molecule and the graphite basal plane.[19] Charge transfer between compounds non-covalently bonded to CNTs has been studied both theoretically[20] and experimentally by observing modification of the electronic[13,21] and opto-electronic properties of CNTFETs.[22,23] As the technical groundwork for producing hybrid CNT structures has been established the challenge of understanding these increasingly complex systems can be addressed.

Buckminsterfullerene (C_{60}) and other closely related carbon allotropes have excellent electron accepting properties for use in organic photo-voltaic devices.[24] Furthermore these molecules can be used as protective cages encapsulating atoms of a wide range of elements. Measurements of exceptionally long spin coherence times in these endohedral fullerene molecules,[25] have led to proposals for their utilization as individual spin qubits, the basic building block of a quantum computer.[26] However, electronically addressing anything but large ensembles of fullerene molecules remains challenging. The use of carbon nanotubes as conducting scaffolds for few or even individual molecules shows great potential for exciting advances in molecular electronics.[17] Composite systems in which fullerenes interact non-covalently with the sidewalls of CNTs without any intermediary have been developed with potential applications in solar cell technology.[27,28] There has also already been some success in attaching C_{60} to SWCNTs *via*

[a]*Department of Materials, University of Oxford, Parks Road, Oxford, OX1 3PH, UK. E-mail: christopher.allen@materials.ox.ac.uk*

[b]*Center for Nanochemistry, College of Chemistry and Molecular Engineering, Peking University, Beijing 100871, P. R. China*

† Electronic supplementary information (ESI) available: AFM line scans of the substrate before and after functionalization; scheme for measuring amorphous carbon coverage from TEM images; diameter comparisons of ac-TEM image and simulation of C_{60} molecule; Raman spectra D peak comparison; optical response of transfer properties of pristine devices; comparison between swept and pulsed V_g measurements; functionalization effect and optical response of the transfer characteristics of a 550 nm and a 450 nm CNTFET device. See DOI: 10.1039/c3nr04314b

non-covalent π–π interactions using various aromatic mediators including pyrene.[29,30] Evidence of photo-induced charge transfer between the C_{60} molecule and SWCNT has been demonstrated *via* optical[31–34] and electronic measurements.[35]

In this work we experimentally investigate the nature of charge transfer in a SWCNT–C_{60} hybrid system. Using a non-covalent π–π interaction we attach *N*-methyl-2-pyrenyl-C_{60} (Pyr-C_{60}) molecules to CNTFET devices and observe signatures of optically activated charge transfer between the carbon nanotube and Pyr-C_{60}.

Experimental

Ultra-long SWCNTs were grown by flow directed chemical vapor deposition onto a heavily doped SiO_2/Si substrate using a $Fe(OH)_3$ or $FeCl_3$ catalyst.[36] FET devices with Cr/Au electrodes were fabricated using standard electron beam lithography techniques and thermal evaporation. By using ultra-long carbon nanotubes we have been able to pattern multiple FET devices onto a single tube (Fig. 1a and b).

Completed FET devices were wire bonded into a ceramic chip holder and electronic measurements performed in ambient conditions using a HP4142B modular DC source/monitor unit. Devices were screened *via* their electronic properties to locate semiconducting tubes. These were then functionalized by drop-casting a solution of 1.25×10^{-4} M *N*-methyl-2-pyrenyl-C_{60} (Fig. 1c)[37] in toluene onto the chip and allowing to dry in air. A schematic of a completed, functionalized device is shown in Fig. 1d.

Atomic force microscopy images were recorded in tapping mode using a Park Scientific CP-II. Raman spectroscopy was performed using a Horiba Jobin Yvon LabRam Aramis system with 532 nm excitation wavelength.

The carbon nanotubes used for the TEM studies were FH-P nanotubes obtained from Meijo Nanocarbon. They were dispersed by sonication in 1,2-dichloroethane for 20 minutes. Two drops of this solution were then applied to lacey carbon TEM grids.

TEM images were recorded at 80 keV using either a JEOL 2010 or Oxfords aberration corrected JEOL 2200 MCO.

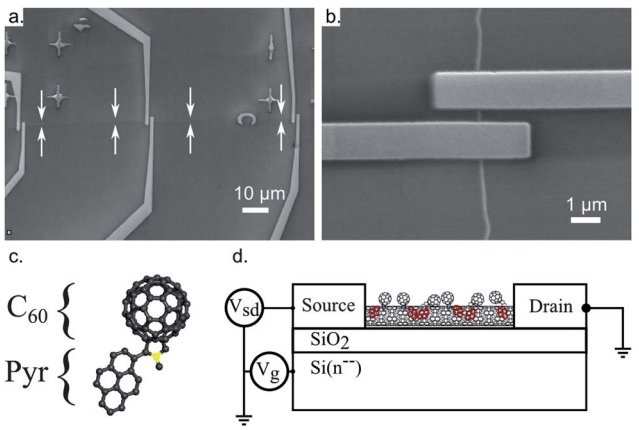

Fig. 1 (a) Scanning electron microscopy (SEM) image of three devices with varying electrode spacing fabricated on an individual ultra-long SWCNT (indicated with arrows). (b) Magnified SEM image of an individual device with electrode spacing ~450 nm. (c) Molecular structure of *N*-methyl-2-pyrenyl-C_{60} with the fullerene (C_{60}) and pyrene group (Pyr) indicated. The yellow sphere represents a nitrogen atom. (d) Schematic of the device geometry after functionalization with the Pyr-C_{60} moiety (pyrene groups highlighted in red). A SWCNT nanotube is contacted by Au/Cr source and drain electrodes. The heavily doped silicon substrate is used as a back-gate.

Results and discussion

Atomic force microscopy

AFM scans of a completed CNTFET device prior to functionalization are shown in Fig. 2a and c. Line profiles across the

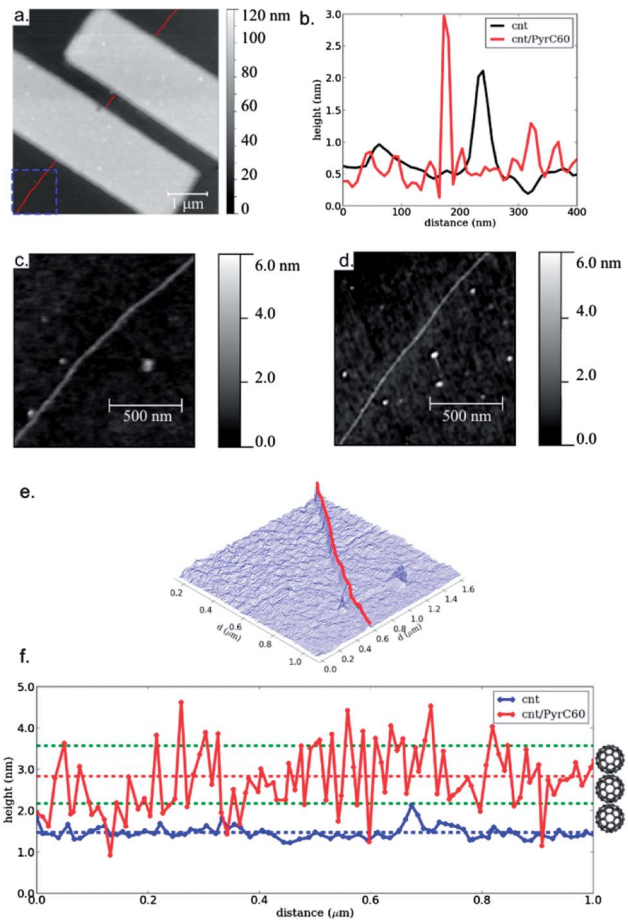

Fig. 2 (a) Atomic force microscopy (AFM) image of a completed CNTFET device. The carbon nanotube is highlighted in red. (b) Line profile across the SWCNT before (black trace) and after (red trace) functionalization with the Pyr-C_{60} moiety. (c) Magnified AFM image of the region highlighted with a blue box in (a) before and (d) after functionalization. (e) AFM topography of the pristine tube displayed as line-scans. The location of maximum tube height for each line-scan is indicated in red. (f) Height as a function of distance along the tube (heights measured at the positions indicated by the red line in (e)) for the pristine (blue) and functionalized (red) SWCNT. The red and blue dashed lines show the mean heights. The green dashed lines mark an increase of one (0.7 nm) and two (2.1 nm) C_{60} diameters on the mean pristine tube height.

pristine tube (Fig. 2b, black trace) give a mean height of 1.5 ± 0.1 nm, confirming the individual single wall nature of this tube. After the addition of the Pyr-C_{60} group (Fig. 2c) the apparent height of the SWCNT was measured as 2.8 ± 0.1 nm (Fig. 2b, red trace) an increase of ~1.3 nm compared to the pristine device. This increase is almost twice the theoretical C_{60} diameter of 0.71 nm.[38] AFM measurements of C_{60} molecules self-assembled in hexagonal close-packed mono- and bi-layers have been measured to have apparent heights of ~1 nm and ~2 nm respectively.[39]

Insight into the degree of coverage achieved by functionalization can be gained by examining how apparent height varies along the tube. The height of the SWCNT was extracted from every line-scan in each of the AFM images (Fig. 2e, red line). The height of the pristine tube (Fig. 2f, blue trace) is fairly consistent across the entire AFM image with a standard deviation of σ = 0.16 nm, comparable with the substrate roughness of 0.15 nm (see ESI, Fig. S1†). The functionalized tube (Fig. 2f, red trace) is considerably rougher with standard deviation of σ = 0.78 nm and measured heights ranging from that of the pristine tube to over 4 nm. This inconsistency in measured height indicates incomplete coverage of the SWCNT by the Pyr-C_{60} moiety with some sections of the tube remaining pristine and others having a covering of thickness equivalent to over three times the diameter of a C_{60} molecule.

Analysis of the AFM data also allows us to comment on the selectivity of the deposition of the Pyr-C_{60} moiety to the CNT. After drop-casting Pyr-C_{60} in toluene on the device, the roughness of the Si substrate doubled from 0.15 nm to 0.30 nm (see ESI, Fig. S1†) indicating that some material has been deposited on the substrate. This is, however less than a quarter of the increase in roughness measured along the tube illustrating the preferential attachment of the Pyr-C_{60} groups to the SWCNT due to the relatively strong π–π bonding. Due to the finite size of the AFM tip used to image the SWCNT device it is not possible to get lateral resolution of the order necessary to resolve individual C_{60} molecules.

Transmission electron microscopy

Fig. 3a–c show high resolution transmission electron microscopy (HRTEM) images of individual or small bundles of pristine SWCNTs and double-wall carbon nanotubes (DWCNTs). All TEM images were recorded at an accelerating voltage of 80 keV, below the threshold for knock on damage in carbon nanotubes.[40] Small amounts of amorphous material can be seen on the tube surfaces, a residue of the growth or dispersion procedures. Fig. 3d–g show HRTEM images of individual SW- and DWCNTs after functionalization with Pyr-C_{60} showing a high degree of coverage with amorphous material. Careful inspection of Fig. 3d–g reveals numerous circular projections with diameters of ~1 nm (highlighted with red arrows in Fig. 3f) on the surface of the CNTs. We interpret these as projections of individual C_{60} molecules. The unambiguous determination of the presence of C_{60} molecules from HRTEM images is challenging as the presence of amorphous material complicates the interpretation. Fullerene molecules can react with neighbouring

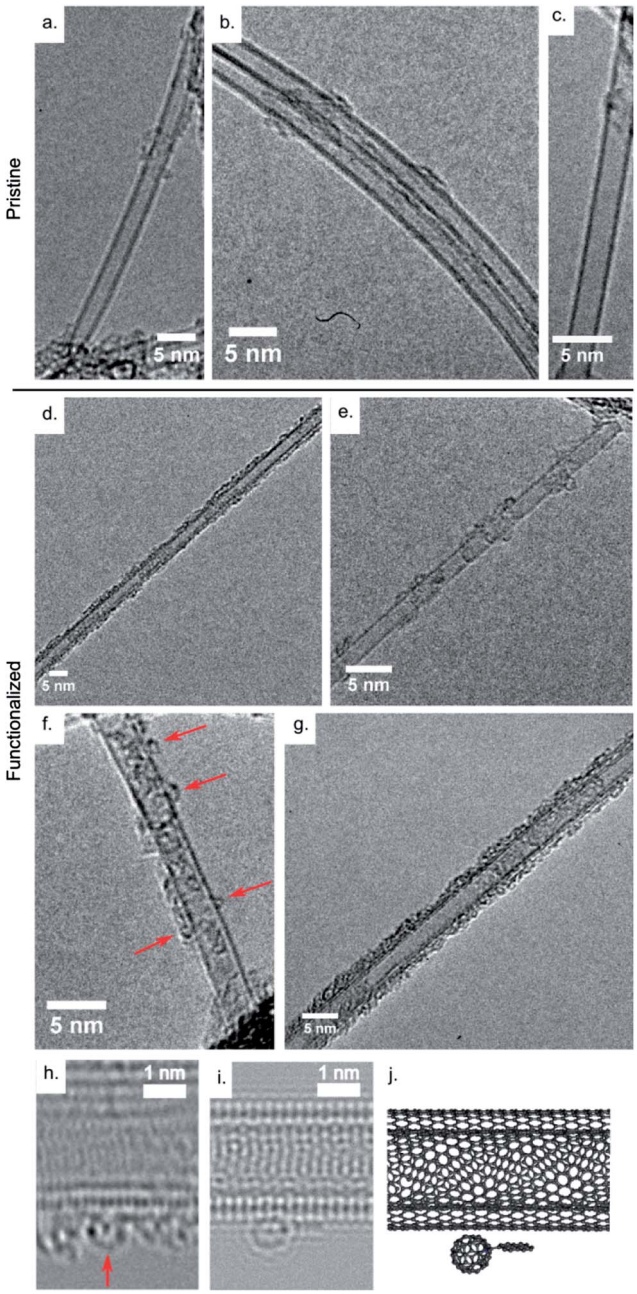

Fig. 3 (a–c) HRTEM images of individual or small bundles of pristine SW- and DWCNTs. (d–g) HRTEM images of individual SW- and DWCNTs after functionalization with Pyr-C_{60}. Red arrows in (f) indicate C_{60}. (h) ac-TEM image and (i) simulated ac-TEM image of a Pyr-C_{60} moiety (indicated by the red arrow) attached to the side of a double-wall carbon nanotube. (j) Atomic model used in the TEM simulation.

species under irradiation from an electron beam,[41,42] further complicating the imaging of these structures. To confirm the presence of C_{60} molecules on the surface of the CNTs we have performed aberration corrected high resolution transmission electron microscopy (ac-HRTEM) of the functionalized tubes.

Fig. 3h shows an ac-HRTEM image of a DWCNT after functionalization with the Pyr-C_{60} moiety. There is significant amorphous material on the surface of the DWCNT. Highlighted with a red arrow is a structure which we interpret as a C_{60}

molecule. Fig. 3i shows an ac-HRTEM image simulation of the Pyr-C_{60} molecule adsorbed on the surface of a DWCNT, and Fig. 3j the atomic model used to create the simulation. In both the simulated and experimental image the projection of C_{60} molecule appears as a circular form with pronounced dark spots on its perimeter and a single dark spot at its centre. Line scans across the experimental and simulated images of the C_{60} molecules (ESI, Fig. S2†) give apparent diameters of 0.71 ± 0.05 nm and 0.68 ± 0.05 nm respectively. This good agreement provides strong evidence to support our interpretation.

Raman spectroscopy

The Raman G band spectra from the pristine SWCNT are shown in Fig. 4a. Raman spectra were recorded across the device (scan positions are shown in Fig. 4e) with the signal intensity corresponding to the area of exposed SWCNT. We could not resolve the radial breathing mode of the Raman spectra for this device. The Raman spectra shows a split G peak with a double-Lorentzian line shape as would be expected for a semiconducting SWCNT (Fig. 4b). The G peak of a semiconducting SWCNT comprises two dominant components, labeled G^- and G^+ corresponding to circumferential and axial vibrations respectively. We can estimate the tube diameter from the relative positions of the split G peak using the simple relationship proposed by Jorio *et al.*[43] $\omega_{G^-} = \omega_{G^+} - C/d_t^2$, with ω_{G^-} and ω_{G^+} correspond to the frequency of the G^- and G^+ peaks respectively. C is a constant which for semiconducting tubes takes the value of 47.7 cm^{-1} and d_t is the tube diameter. Lorentzian fits to the two dominant G peaks in the Raman spectra of the pristine tube (Fig. 4b) give peak positions of $\omega_{G^+} = 1591.7$ cm^{-1} and $\omega_{G^-} = 1576.5$ cm^{-1}. From this we estimate a tube diameter of $d_t \sim 1.8$ nm, somewhat larger than previously measured by AFM.

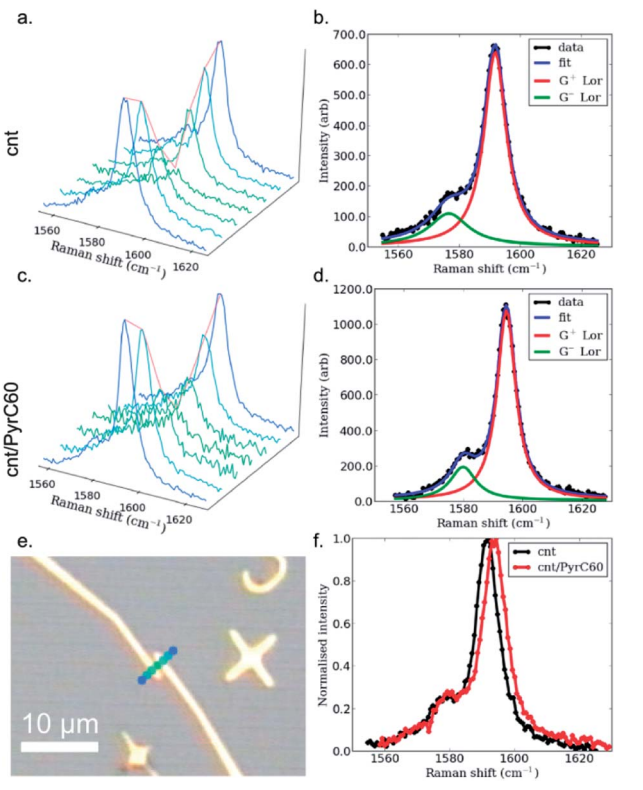

Fig. 4 (a) Raman spectra of the G peak of the pristine carbon nanotube with trace colors corresponding to the scan positions indicated in the optical image shown in (e). (b) Double Lorentzian fit to the G peak of the Raman spectra from the pristine tube. (c) Raman spectra of the G peak of the carbon nanotube after functionalization with the Pyr-C_{60} moiety and (d) fit to the G peak. (f) Comparison between the normalized G peak Raman spectra of the pristine (black) and functionalized (red) SWCNT.

The position of Raman G^+ band of a semiconducting SWCNT is related to its Fermi level due to strong electron-phonon coupling in resonant Raman spectroscopy.[44] It is therefore possible to detect doping *via* Raman spectroscopy of graphitic structures. Indeed, shifts in the position of the G^+ band with chemical doping have been reported in Raman studies of intercalated graphite,[45] carbon nano-horns[46] and nanotubes[47,48] with hole doping causing a small blue shift in ω_{G^+} and electron doping a small red shift.

The Raman spectra of the device after functionalization with Pyr-C_{60} are shown in Fig. 4c. Lorentzian fits give peak positions of $\omega_{G^+} = 1594.4$ cm^{-1} and $\omega_{G^-} = 1578.5$ cm^{-1} (Fig. 4d), a blue shift of the G^+ peak by $\Delta\omega_{G^+} = +2.7$ cm^{-1} (Fig. 4f). This shift in ω_{G^+} with functionalization corresponds to electron transfer from the SWCNT to the attached Pyr-C_{60} moieties, resulting in hole doping of the tube. Raman studies of electrostatic doping of SWCNTs have found shifts in the G^+ peak of $\Delta\omega_{G^+} \sim +3$ cm^{-1} for a decrease in charge density of ~0.4 e.nm^{-1}.[49] We therefore tentatively estimate a charge transfer from the SWCNT to Pyr-C_{60} of ~0.36 e nm^{-1}.

Within the spatial resolution of this measurement (laser spot size ~1 μm), the position of the G peak is consistent across the device and there is no appreciable increase in the amplitude of the disorder related D peak with functionalization (ESI, Fig. S3a†). No shift in G peak position was seen on treatment of CNTFET devices with the toluene solvent (ESI, Fig. S3b†).

Electronic measurements

Fig. 5a shows the transfer characteristics of a CNTFET device with channel length of ~250 nm before and after functionalization with the Pyr-C_{60} moiety The pristine device (black curve) shows p-type semiconducting behavior typical of CNTFETs measured in ambient conditions,[50] and hysteresis due to accumulation of charge in response to the application of the gate voltage.[51]

After functionalization with the Pyr-C_{60} moiety (Fig. 5a, blue curve) there is a change in the device transfer characteristics. In order to identify the mechanism underlying this change we concentrate on three key parameters shown schematically in Fig. 5b. Firstly the transconductance, dI/dV_g, of a FET is related to the mobility of the device, the height of any Schottky barrier between the electrodes and carbon nanotube and the capacitive coupling to the gate electrode. Secondly, the gate voltage at which the device is turned on, the threshold voltage V_{th}, is a consequence of the band alignment between electrode and carbon nanotube. Finally, the on-state conductance of the device, $G_{on} = I_{on}/V_{sd}$, is determined by the sum of the contact resistances and the channel resistance.

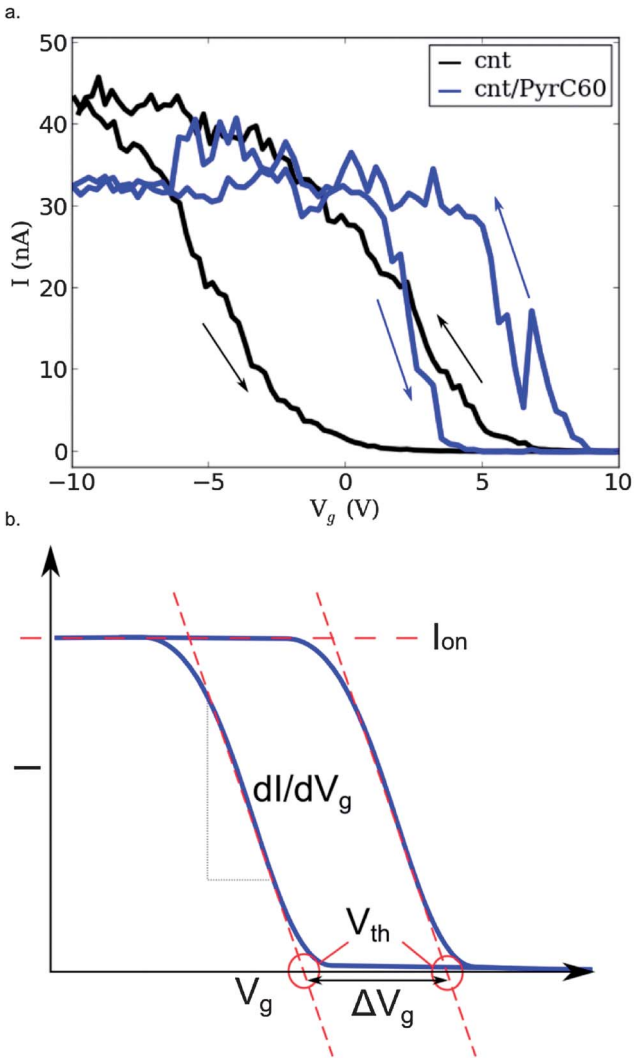

Fig. 5 (a) Transfer characteristics of a semiconducting CNTFET device before (black) and after (blue) functionalization measured with a bias voltage of $V_{sd} = 50$ mV. The arrows denote the sweep direction. (b) Schematic transfer curve with definitions of trans-conductance (dI/dV_g), threshold voltage (V_{th}), on-state current (I_{on}) and hysteresis width (ΔV_g) marked.

On functionalization there is a small drop in the on-state conductance from $G^{p}_{on} \sim 8.6$ μS in the pristine CNTFET device to $G^{f}_{on} \sim 6.5$ μS. There is also an increase in the trans-conductance of the device from which the device field-effect mobility can be calculated using[52]

$$\mu_{FE} = \frac{1}{V_{sd}} \frac{dI}{dV_g} \left(\frac{L^2}{C} \right) \quad (1)$$

with L the channel length and C the gate capacitance of the device given by

$$C = \frac{2\pi\varepsilon_0\varepsilon L}{\ln\left(\frac{4t_{ox}}{d_t}\right)} \quad (2)$$

$\varepsilon = 2.45$ is the average of the dielectric constant of silicon ($\varepsilon = 3.9$) and air ($\varepsilon = 1$), $t_{ox} = 300$ nm the oxide thickness and $d_t = 1.7$ nm the tube diameter. After functionalization the peak field-effect mobility almost doubles from $\mu^{p}_{FE} = 20.7$ cm^2 V^{-1} s^{-1} in the pristine device to $\mu^{f}_{FE} = 37.7$ cm^2 V^{-1} s^{-1}. There is a clear shift in the transfer curve to more positive V_g with the up sweep threshold voltage shifting from $V^{p}_{th,u} = -2.2$ V for the pristine SWCNT device to $V^{f}_{th,u} = +4.7$ V after functionalization, a shift of $\delta V_{th,u} = +6.9$ V. Similarly the down sweep threshold voltage changes from $V^{p}_{th,d} = +5.7$ V for the pristine device to $V^{f}_{th,d} = +8.4$ V post functionalization, a shift of $\delta V_{th,d} = +2.7$ V. There is an appreciable reduction in the transfer hysteresis with functionalization from $\Delta V^{p}_{g} = 7.9$ V to $\Delta V^{f}_{g} = 3.7$ V.

The effect of functionalization on the transfer characteristics of a CNTFET has been addressed in detail by Heller *et al.*[5] Here we will consider the possible physical mechanism behind each of the observed changes individually. Firstly the drop in on-state conductance with functionalization is attributed to an increase in scattering along the carbon nanotube after attachment of the Pyr-C_{60} molecule. Secondly, the increase in transconductance dI/dV_g can be explained in terms of a decrease in Schottky barrier height for hole conduction between the electrodes and SWCNT caused by the local modification of work-function at the electrode-SWCNT interface.[53] Finally, the observed shift in threshold voltage δV_{th} can be understood in terms of the transfer of charge from the SWCNT to the Pyr-C_{60} molecule modifying the Fermi level in the conduction channel thus altering the gate voltage required for full carrier depletion, effectively hole-doping the device.

We can make a simple estimation of the change in carrier density (in this case holes) on our device from the measurement of δV_{th}.[52] The change in charge on the CNTFET can be written $\delta Q = C\delta V_{th}$ and the corresponding change in carrier density $\delta p = \delta Q/eL$. For our device with estimated capacitance of $C = 4.9 \times 10^{-18}$ F, channel length of $L = 250$ nm and $\delta V_{th,u} = +6.9$ V ($\delta V_{th,d} = +2.7$ V) we calculate an increase in carrier density of $\delta p_u = 0.85$ nm^{-1} ($\delta p_d = 0.33$ nm^{-1}) or the addition of 212 (83) holes to the 250 nm long CNTFET device. This maximum change in charge density of 0.85 nm^{-1} is over twice that estimated from the G^+ peak shift in the Raman data.

A similar conclusion has been reached by Shen *et al.* to explain the combined p doping and drop in on-state conductance in composite CNT–C_{60} FET devices.[35] Other studies on the effect of molecules adsorbed onto the surface of CNTFET devices have estimated charge transfer of 0.04 electrons per NH_3 molecule,[14] 0.37 electrons per porphyrin molecule[22] and 2.2 electrons per pyrene-CdSe moiety.[23]

The decrease in hysteresis of $\Delta V^{p}_{g} - \Delta V^{f}_{g} = 2.5$ V in the transfer curve after functionalization suggests that the Pyr-C_{60} molecule is to some extent displacing other surface mobile species which screen the applied gate voltage.

Fig. 6 shows the change in transfer characteristics of the device when measured in the dark and under illumination with white light (150 W halogen bulb). The peak mobility of the device is unchanged upon illumination (44.1 cm^2 V^{-1} s^{-1} in the dark and 44.3 cm^2 V^{-1} s^{-1} under illumination). The threshold voltage shifts from $V^{up,d}_{th} = 3.9$ V to $V^{up,l}_{th} = 5.2$ V on the up sweep, a shift of $\delta V^{up}_{th} = 1.3$ V, corresponding to the addition of ~40 holes to the device or an increase in hole density of ~0.16 nm^{-1}.

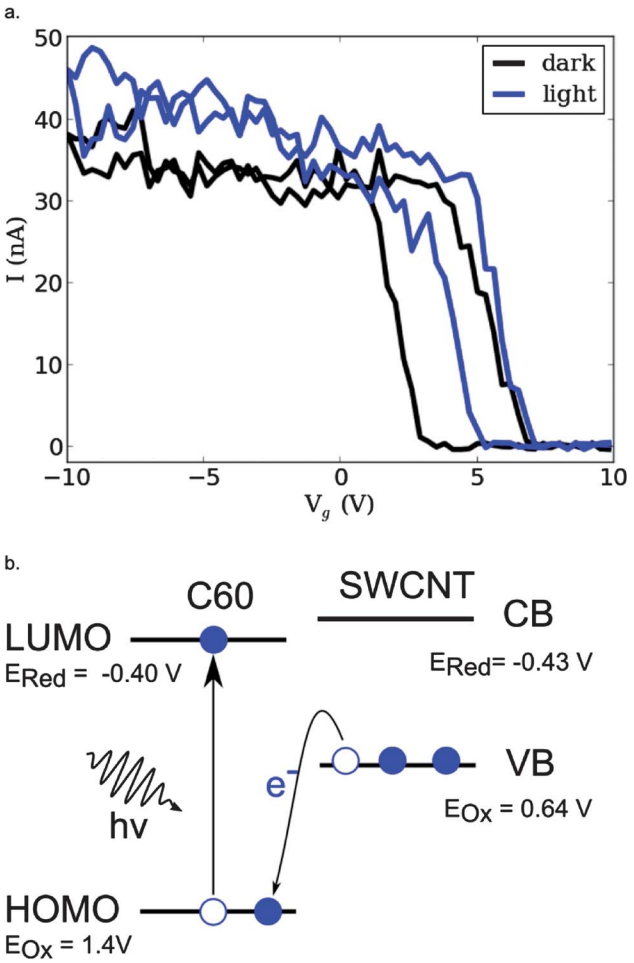

Fig. 6 (a) Transfer characteristics of a functionalized carbon nanotube FET measured in the dark (black curve) and under illumination from a 150 W halogen lamp (blue curve). (b) Schematic energy level diagram for the optically activated charge separation process with redox potentials for a (6,5) SWCNT marked.[58]

The change in threshold voltage for the down sweep is considerably less ($V_{th}^{down,d} = 6.9$ V, $V_{th}^{down,l} = 70$ V, $\delta V_{th}^{down} = 0.1$ V). We also observe a significant reduction in the transfer hysteresis of the device from $\Delta V_g^d = 3.0$ V when measured in the dark to $\Delta V_g^l = 1.8$ V under illumination, a reduction of ~1.2 V. There was no appreciable change in the transfer characteristics of the pristine device with illumination (see ESI, Fig. S4†).

Previous reports on similar Pyr-C_{60}–SWCNT systems have explained photo-excited charge separation in terms of interactions between the host SWCNT and attached C_{60} molecules.[31] It is, however, important to consider the role of the pyrene molecule in any observed effect,[54] particularly any optical response.[55,56] In order to determine the degree to which the response of our Pyr-C_{60}–SWCNT system is due to just the pyrene molecule control experiments were performed in which SWCNT–FET devices were functionalized with ~1.5 M pyrene in toluene. We observed a small negative shift of V_{th} on functionalization and no discernable optical response (see ESI, Fig. S5†). We therefore ascribe the optical enhancement of the doping effect to interactions between the host SWCNT and C_{60} molecule.

The mechanism of photo-excited charge separation in Pyr-C_{60}–SWCNT hybrid systems (shown schematically in Fig. 6b) has been determined from optical measurements.[31] The photo-excitation of an electron from the highest-occupied molecular orbital (HOMO) to the lowest unoccupied molecular orbital (LUMO) in the C_{60} molecule allows an electron from the valence band of the SWCNT to hop into the vacant C_{60} HOMO state. This leaves the SWCNT hole doped and causes the shift to more positive V_g observed in our CNTFET measurements. As this mechanism is dependent on the precise band alignment between the SWCNT and C_{60} molecule it is sensitive to the size of the band-gap in the semiconducting SWCNT and thus the tube chirality.[57]

Fig. 7a shows the reproducibility of the photo-switching process. In order to minimize hysteresis these measurements

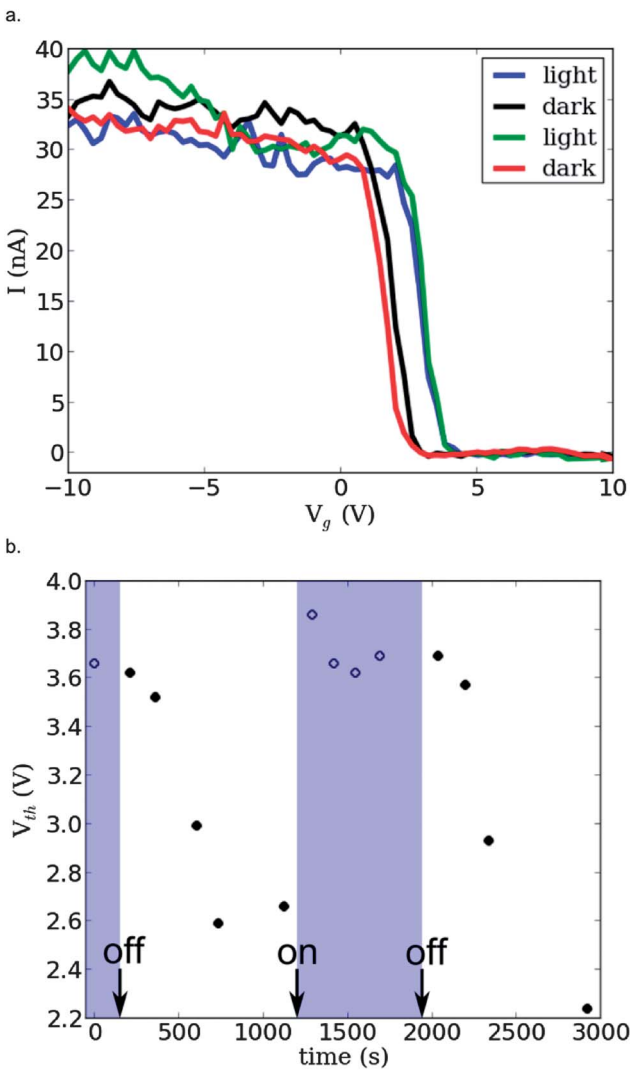

Fig. 7 (a) Transfer characteristics of the functionalized CNTFET device measured over repeated dark–light cycles (only the up sweep is shown for clarity). (b) Variation of threshold voltage (V_{th}) with time from transfer curve measurements under illumination and in the dark. The shaded regions correspond to periods of illumination and the white regions to periods of dark.

were performed using a pulsed gate technique (see ESI, Fig. S6a†)[59] and we only show the up sweep for clarity (representative full hysteresis curves are shown in ESI, Fig. S6b†). There is a reproducible threshold voltage shift from V_{th} ~3.7 V in the illuminated case to V_{th} ~2.5 V in the dark, a change of $\delta V_{th} = 1.2$ V, equivalent to that measured with the standard gate voltage sweep (Fig. 6a). Between each 'light' and 'dark' measurement shown in Fig. 7a the device was allowed to settle for approximately 15 minutes.

Fig. 7b shows the measured threshold voltages from pulsed gate measurements of the SWCNT–Pyr-C_{60} device as a function of time. The shaded regions correspond to periods of illumination and the times at which the halogen lamp was turned on and off are marked. During periods of illumination the measured V_{th} remains stable to within ± 0.2 V. Transfer curves measured immediately after the lamp is turned off show little discernible change in V_{th}. When measured after increasingly long periods in the dark V_g shifts towards lower values, plateauing at around 2.5 V. This observed behavior suggests that the charge transfer from the SWCNT to the C_{60} molecule which occurs on illumination is significantly faster than the transfer of charge back to the nanotube. This increase in time to recover the un-illuminated state is in qualitative agreement with other studies[22,23] with persistent charge separation decay times as long as 1.8×10^3 s having been reported in functionalized SWCNT systems.[60]

Similar results were obtained from devices with 450 nm and 500 nm channel length fabricated on the same SWCNT as those presented in Fig. 5–7 (see ESI, Fig. S7 and S8†). However due to the inferior quality of the data we were unable to reliably extract doping densities.

Conclusions

In this work we have successfully incorporated fullerene molecules into CNTFET devices. Structural characterization has confirmed the presence of C_{60} molecules and the preferential nature of their attachment to the graphitic lattice of the carbon nanotubes.

Through the change in Raman spectra and room temperature transport properties we have demonstrated charge transfer from individual SWCNTs to attached Pyr-C_{60} moieties. The absorbance of Pyr-C_{60} onto the surface a semiconducting SWCNT caused four distinct changes to the CNTFET transfer characteristics which can each be physical rationalized:

1. A small decrease in on state current after functionalization indicated an increase in scattering in the CNTFET conduction channel.

2. An increase in trans-conductance was attributed to a decrease in the SWCNT–electrode Schottky barrier height.

3. A shift in the threshold voltage can be explained in terms of hole doping of the carbon nanotube by the adsorbed Pyr-C_{60} molecule.

4. The decrease in device hysteresis was due to the displacement of other surface species by the adsorption of Pyr-C_{60} moieties onto the surface of the SWCNT.

The increase in density of holes after functionalization was found to be up to 0.85 nm^{-1}. Due to the band alignment between C_{60} and the semiconducting SWCNT we were able to demonstrate optically excited charge transfer between the Pyr-C_{60} and SWCNT causing further hole doping of the device by an additional 0.16 nm^{-1}.

We have demonstrated the feasibility of using electronic measurements to probe interactions between a SWCNT and exohedrally attached C_{60} molecules. This approach should be directly transferable to the wide range of endohedral metallofullerenes allowing for the study of the electronic states of exotic spin-active hybrid systems. Furthermore, by tailoring the size of the aromatic anchor group, it should be possible to control the density of C_{60} molecules decorating the SWCNT.

Acknowledgements

This work was supported by EPSRC (EP/H001972/1) and MOST (2011CB932601).

Notes and references

1 M. S. Dresselhaus, G. Dresselhaus, J. C. Charlier and E. Hernández, Electronic, Thermal and Mechanical Properties of Carbon Nanotubes, *Philos. Trans. R. Soc., A*, 2004, **362**, 2065–2098.
2 P. Avouris, Z. Chen and V. Perebeinos, Carbon-Based Electronics, *Nat. Nanotechnol.*, 2007, **2**, 605.
3 M. P. Anantram and F. Leonard, Physics of Carbon Nanotube Electronic Devices, *Rep. Prog. Phys.*, 2006, **69**, 507–561.
4 T. Umeyama and H. Imahori, Photofunctional Hybrid Nanocarbon Materials, *J. Phys. Chem. C*, 2013, **117**, 3195–3209.
5 I. Heller, A. M. Janssens, J. Männik, E. D. Minot, S. G. Lemay and C. Dekker, Identifying the Mechanism of Biosensing With Carbon Nanotube Transistors, *Nano Lett.*, 2008, **8**, 591–595.
6 J. Kong, Nanotube Molecular Wires as Chemical Sensors, *Science*, 2000, **287**, 622–625.
7 M. E. Roberts, M. C. LeMieux and Z. Bao, Sorted and Aligned Single-walled Carbon Nanotube Networks for Transistor-based Aqueous Chemical Sensors, *ACS Nano*, 2009, **3**, 3287–3293.
8 K. Bradley, M. Briman, A. Star and G. Grüner, Charge Transfer from Adsorbed Proteins, *Nano Lett.*, 2004, **4**, 253–256.
9 M. Bockrath, J. Hone, A. Zettl, P. McEuen, A. Rinzler and R. Smalley, Chemical Doping of Individual Semiconducting Carbon-nanotube Ropes, *Phys. Rev. B: Condens. Matter Mater. Phys.*, 2000, **61**, R10606–R10608.
10 C. Klinke, J. Chen, A. Afzali and P. Avouris, Charge Transfer Induced Polarity Switching in Carbon Nanotube Transistors, *Nano Lett.*, 2005, **5**, 555–558.
11 B. R. Kang, W. J. Yu, K. K. Kim, H. K. Park, S. M. Kim, Y. Park, G. Kim, H.-J. Shin, U. J. Kim, E.-H. Lee, *et al.*, Restorable Type Conversion of Carbon Nanotube Transistor Using

Pyrolytically Controlled Antioxidizing Photosynthesis Coenzyme, *Adv. Funct. Mater.*, 2009, **19**, 2553–2559.
12 C. Klinke, A. Afzali and P. Avouris, Interaction of Solid Organic Acids with Carbon Nanotube Field Effect Transistors, *Chem. Phys. Lett.*, 2006, **430**, 75–79.
13 A. Star, T.-R. Han, J.-C. Gabriel, K. Bradley and G. Grüner, Interaction of Aromatic Compounds with Carbon Nanotubes: Correlation to the Hammett Parameter of the Substituent and Measured Carbon Nanotube FET Response, *Nano Lett.*, 2003, **3**, 1421–1423.
14 K. Bradley, J.-C. Gabriel, M. Briman, A. Star and G. Grüner, Charge Transfer from Ammonia Physisorbed on Nanotubes, *Phys. Rev. Lett.*, 2003, **91**, 218301.
15 D. Tasis, N. Tagmatarchis, A. Bianco and M. Prato, Chemistry of Carbon Nanotubes, *Chem. Rev.*, 2006, **106**, 1105–11036.
16 R. J. Chen, Y. Zhang, D. Wang and H. Dai, Noncovalent Sidewall Functionalization of Single-walled Carbon Nanotubes for Protein Immobilization, *J. Am. Chem. Soc.*, 2001, **123**, 3838–3839.
17 M. Urdampilleta, S. Klyatskaya, J.-P. Cleuziou, M. Ruben and W. Wernsdorfer, Supramolecular Spin Valves, *Nat. Mater.*, 2011, **10**, 502–506.
18 K. A. Shiral Fernando, Y. Lin, W. Wang, S. Kumar, B. Zhou, S.-Y. Xie, L. T. Cureton and Y.-P. Sun, Diminished Band-gap Transitions of Single-walled Carbon Nanotubes in Complexation with Aromatic Molecules, *J. Am. Chem. Soc.*, 2004, **126**, 10234–10235.
19 C. A. Hunter and J. K. M. Sanders, The Nature of π–πInteractions, *J. Am. Chem. Soc.*, 1990, **112**, 5525–5534.
20 J. Zhao, J. P. Lu, J. Han and C.-K. Yang, Noncovalent Functionalization of Carbon Nanotubes by Aromatic Organic Molecules, *Appl. Phys. Lett.*, 2003, **82**, 3746.
21 A. Wurl, S. Goossen, D. Canevet, M. Sallé, E. M. Pérez, N. Martín and C. Klinke, Supramolecular Interaction of Single-Walled Carbon Nanotubes with a Functional TTF-Based Mediator Probed by Field-Effect Transistor Devices, *J. Phys. Chem. C*, 2012, **116**, 20062–20066.
22 D. S. Hecht, R. J. A. Ramirez, M. Briman, E. Artukovic, K. S. Chichak, J. F. Stoddart and G. Grüner, Bioinspired Detection of Light Using a Porphyrin-Sensitized Single-Wall Nanotube Field Effect Transistor, *Nano Lett.*, 2006, **6**, 2031–2036.
23 L. Hu, Y.-L. Zhao, K. Ryu, C. Zhou, J. F. Stoddart and G. Grüner, Light-Induced Charge Transfer in Pyrene/CdSe–SWNT Hybrids, *Adv. Mater.*, 2008, **20**, 939–946.
24 C.-Z. Li, H.-L. Yip and A. K.-Y. Jen, Functional Fullerenes for Organic Photovoltaics, *J. Mater. Chem.*, 2012, **22**, 4161.
25 J. J. L. Morton, A. M. Tyryshkin, A. Ardavan, K. Porfyrakis, S. A. Lyon and G. A. D. Briggs, Electron Spin Relaxation of N@C_{60} in CS_2, *J. Chem. Phys.*, 2006, **124**, 14508.
26 S. C. Benjamin, A. Ardavan, G. A. D. Briggs, D. A. Britz, D. Gunlycke, J. Jefferson, M. A. G. Jones, D. F. Leigh, B. Lovett, A. N. Khlobystov, *et al.*, Towards a Fullerene-based Quantum Computer, *J. Phys.: Condens. Matter*, 2006, **18**, S867–S883.
27 T. Umeyama, N. Tezuka, S. Seki, Y. Matano, M. Nishi, K. Hirao, H. Lehtivuori, N. V. Tkachenko, H. Lemmetyinen, Y. Nakao, *et al.*, Selective Formation and Efficient Photocurrent Generation of [70]Fullerene-Single-Walled Carbon Nanotube Composites, *Adv. Mater.*, 2010, **22**, 1767–1770.
28 V. C. Tung, J.-H. Huang, I. Tevis, F. Kim, J. Kim, C.-W. Chu, S. I. Stupp and J. Huang, Surfactant-Free Water-Processable Photoconductive All-Carbon Composite, *J. Am. Chem. Soc.*, 2011, **133**, 4940–4947.
29 G. Bottari, D. Olea, V. López, C. Gomez-Navarro, F. Zamora, J. Gómez-Herrero and T. Torres, Ordering phthalocyanine-C60 Fullerene Conjugates on Individual Carbon Nanotubes, *Chem. Commun.*, 2010, **46**, 4692–4694.
30 D. M. Guldi, E. Menna, M. Maggini, M. Marcaccio, D. Paolucci, F. Paolucci, S. Campidelli, M. Prato, G. M. A. Rahman and S. Schergna, Supramolecular Hybrids of [60]fullerene and Single-wall Carbon Nanotubes, *Chem.–Eur. J.*, 2006, **12**, 3975–3983.
31 A. S. D. Sandanayaka, E. Maligaspe, T. Hasobe, O. Ito and F. D'Souza, Diameter Dependent Electron Transfer in Supramolecular Nanohybrids of (6,5)- or (7,6)-Enriched Semiconducting SWCNT as Donors and Fullerene as Acceptor, *Chem. Commun.*, 2010, **46**, 8749–8751.
32 F. D'Souza, R. Chitta, A. S. D. Sandanayaka, N. K. Subbaiyan, L. D'Souza, Y. Araki and O. Ito, Supramolecular Carbon Nanotube-Fullerene Donor–Acceptor Hybrids for Photoinduced Electron Transfer, *J. Am. Chem. Soc.*, 2007, **129**, 15865–15871.
33 F. D'Souza and O. Ito, Photosensitized Electron Transfer Processes of Nanocarbons Applicable to Solar Cells, *Chem. Soc. Rev.*, 2012, **41**, 86–96.
34 F. D'Souza, S. K. Das, A. S. D. Sandanayaka, N. K. Subbaiyan, D. R. Gollapalli, M. E. Zandler, T. Wakahara and O. Ito, Photoinduced Charge Separation in Three-Layer Supramolecular Nanohybrids: Fullerene–Porphyrin–SWCNT, *Phys. Chem. Chem. Phys.*, 2012, **14**, 2940–2950.
35 Y. Shen, J. S. Reparaz, M. R. Wagner, A. Hoffmann, C. Thomsen, J.-O. Lee, S. Heeg, B. Hatting, S. Reich, A. Saeki, *et al.*, Assembly of Carbon Nanotubes and Alkylated Fullerenes: Nanocarbon Hybrid Towards Photovoltaic Applications, *Chem. Sci.*, 2011, **2**, 2243.
36 Y. Yao, X. Dai, C. Feng, J. Zhang, X. Liang, L. Ding, W. Choi, J.-Y. Choi, J. M. Kim and Z. Liu, Crinkling Ultralong Carbon Nanotubes into Serpentines by a Controlled Landing Process, *Adv. Mater.*, 2009, **21**, 4158–4162.
37 G. Liu, A. N. Khlobystov, A. Ardavan, G. A. D. Briggs and K. Porfyrakis, Photochemical Stability of N@C_{60} and Its Pyrrolidine Derivatives, *Chem. Phys. Lett.*, 2011, **508**, 187–190.
38 W. Krätschmer, L. D. Lamb, K. Fostiropoulos and D. R. Huffman, Solid C60: a New Form of Carbon, *Nature*, 1990, **347**, 354–358.
39 S. Burke, J. Mativetsky, R. Hoffmann and P. Grütter, Nucleation and Submonolayer Growth of C60 on KBr, *Phys. Rev. Lett.*, 2005, **94**, 096102.

40 F. Banhart, Irradiation Effects in Carbon Nanostructures, *Rep. Prog. Phys.*, 1999, **62**, 1181–1221.
41 M. Koshino, Y. Niimi, E. Nakamura, H. Kataura, T. Okazaki, K. Suenaga and S. Iijima, Analysis of the Reactivity and Selectivity of Fullerene Dimerization Reactions at the Atomic Level, *Nat. Chem.*, 2010, **2**, 117–124.
42 C. S. Allen, Y. Ito, A. W. Robertson, H. Shinohara and J. H. Warner, Two-Dimensional Coalescence Dynamics of Encapsulated Metallofullerenes in Carbon Nanotubes, *ACS Nano*, 2011, **5**, 10084–10089.
43 A. Jorio, A. Souza Filho, G. Dresselhaus, M. Dresselhaus, A. Swan, M. Ünlü, B. Goldberg, M. Pimenta, J. Hafner, C. Lieber, *et al.*, G-Band Resonant Raman Study of 62 Isolated Single-wall Carbon Nanotubes, *Phys. Rev. B: Condens. Matter Mater. Phys.*, 2002, **65**, 23–27.
44 J. Park, J. Sasaki, R. Saito, W. Izumida, M. Kalbac, H. Farhat, G. Dresselhaus and M. Dresselhaus, Fermi Energy Dependence of the G-Band Resonance Raman Spectra of Single- Wall Carbon Nanotubes, *Phys. Rev. B: Condens. Matter Mater. Phys.*, 2009, **80**, 081402.
45 M. Dresselhaus and G. Dresselhaus, Intercalation Compounds of Graphite, *Adv. Phys.*, 1981, **51**, 1–186.
46 S. Bandow, A. M. Rao, G. U. Sumanasekera, P. C. Eklund, F. Kokai, J. Takahashi, M. Yudasaka and S. Iijima, Evidence for Anomalously Small Charge Transfer in Doped Single-wall Carbon Nanohorn Aggregates with Li, K and Br, *Appl. Phys. A*, 2000, **71**, 561–564.
47 A. Rao, P. Eklund, S. Bandow, A. Thess and R. Smalley, Evidence for Charge Transfer in Doped Carbon Nanotube Bundles from Raman Scattering, *Nature*, 1997, **191**, 257–259.
48 T. Pichler, A. Kukovecz, H. Kuzmany and H. Kataura, Charge Transfer in Doped Single Wall Carbon Nanotubes, *Synth. Met.*, 2003, **135–136**, 717–719.
49 J. C. Tsang, M. Freitag, V. Perebeinos, J. Liu, P. Avouris, Doping and P. Renormalization, Carbon Nanotubes, *Nat. Nanotechnol.*, 2007, **2**, 725–730.
50 P. G. Collins, K. Bradley, M. Ishihami and A. Zettl, Extreme Oxygen Sensitivity of Electronic Properties of Carbon Nanotubes, *Science*, 2000, **287**, 180.
51 Y. Pascal-Levy, E. Shifman, M. Pal-Chowdhury, I. Kalifa, T. Rabkin, O. Shtempluck, A. Razin, V. Kochetkov and Y. Yaish, Water-Assisted Mobile Charge Induced Screening and Origin of Hysteresis in Carbon Nanotube Field-Effect Transistors, *Phys. Rev. B: Condens. Matter Mater. Phys.*, 2012, **86**, 1–9.
52 R. Martel, T. Schmidt, H. R. Shea, T. Hertel and P. Avouris, Single- and Multi-wall Carbon Nanotube Field-effect Transistors, *Appl. Phys. Lett.*, 1998, **73**, 2447–2449.
53 J. Chen, C. Klinke, A. Afzali and P. Avouris, Self-aligned Carbon Nanotube Transistors with Charge Transfer Doping, *Appl. Phys. Lett.*, 2005, **86**, 123108.
54 M. B. Lerner, J. M. Resczenski, A. Amin, R. R. Johnson, J. I. Goldsmith and A. T. C. Johnson, Toward Quantifying the Electrostatic Transduction Mechanism in Carbon Nanotube Molecular Sensors, *J. Am. Chem. Soc.*, 2012, **137**, 14318–14321.
55 Rajesh, T. Sarkar and A. Mulchandani, Photo-Induced Charge Transport in ZnS Nanocrystals Decorated Single Walled Carbon Nanotube Field-Effect Transistor, *Appl. Phys. Lett.*, 2011, **99**, 173110.
56 Y.-L. Zhai and J. F. Stoddart, Noncovalent Functionalization of Single-Walled Carbon Nanotubes, *Acc. Chem. Res.*, 2009, **42**, 1161–1171.
57 C. M. Isborn, C. Tang, A. Martini, E. R. Johnson, A. Ortero-de-la-Roza and V. C. Tung, Carbon Nanotube Chirality Determines Efficiency of Electron Transfer to Fullerene in All-Carbon Photovoltaics, *J. Phys. Chem. Lett.*, 2013, **4**, 2914–2918.
58 Y. Tanaka, Y. Hirana, Y. Niidome, K. Kato, S. Saito and N. Nakashima, Experimentally Determined Redox Potentials of Individual (n,m) Single-Walled Carbon Nanotubes, *Angew. Chem., Int. Ed. Engl.*, 2009, **48**, 7655–7659.
59 D. Estrada, S. Dutta, A. Liao and E. Pop, Reduction of Hysteresis for Carbon Nanotube Mobility Measurements Using Pulsed Characterization, *Nanotechnology*, 2010, **21**, 085702.
60 R. F. Khairoutdinov, L. V. Doubova, R. C. Haddon and L. Saraf, Persistent Photoconductivity in Chemically Modified Single-Wall Carbon Nanotubes, *J. Phys. Chem. B*, 2004, **108**, 19976–19981.

